

# Coexistence of polar displacements and conduction in doped ferroelectrics: an *ab initio* comparative study

Chengliang Xia<sup>1,2</sup>, Yue Chen<sup>1,\*</sup> and Hanghui Chen<sup>2,3,\*</sup>

<sup>1</sup>*Department of Mechanical Engineering,*

*The University of Hong Kong,*

*Pokfulam Road, Hong Kong SAR, China*

<sup>2</sup>*NYU-ECNU Institute of Physics,*

*NYU Shanghai, Shanghai, 200062, China*

<sup>3</sup>*Department of Physics,*

*New York University,*

*New York 10003, USA*

## Abstract

Polar metals are rare because free carriers in metals screen electrostatic potential and eliminate internal dipoles. Degenerate doped ferroelectrics may create an approximate polar metallic phase. We use first-principles calculations to investigate  $n$ -doped LiNbO<sub>3</sub>-type oxides (LiNbO<sub>3</sub> as the prototype) and compare to widely studied perovskite oxides (BaTiO<sub>3</sub> as the prototype). In the rigid-band approximation, substantial polar displacements in  $n$ -doped LiNbO<sub>3</sub> persist even at 0.3  $e/f.u.$  ( $\simeq 10^{21} \text{ cm}^{-3}$ ), while polar displacements in  $n$ -doped BaTiO<sub>3</sub> quickly get suppressed and completely vanish at 0.1  $e/f.u.$  Furthermore, in  $n$ -doped LiNbO<sub>3</sub>, Li-O displacements decay more slowly than Nb-O displacements, while in  $n$ -doped BaTiO<sub>3</sub>, Ba-O and Ti-O displacements decay approximately at the same rate. Supercell calculations that use oxygen vacancies as electron donors support the main results from the rigid-band approximation and provide more detailed charge distributions. Substantial cation displacements are observed throughout LiNbO<sub>3- $\delta$</sub>  ( $\delta = 4.2\%$ ), while cation displacements in BaTiO<sub>3- $\delta$</sub>  ( $\delta = 4.2\%$ ) are almost completely suppressed. We find that conduction electrons in LiNbO<sub>3- $\delta$</sub>  are not as uniformly distributed as in BaTiO<sub>3- $\delta$</sub> , implying that the rigid-band approximation should be used with caution in simulating electron doped LiNbO<sub>3</sub>-type oxides. Our work shows that polar distortions and conduction can coexist in a wide range of electron concentration in  $n$ -doped LiNbO<sub>3</sub>, which is a practical approach to generating an approximate polar metallic phase. Combining doped ferroelectrics and doped semiconductors may create new functions for devices.

## I. INTRODUCTION

Polar metals are materials that are characterized by the absence of inversion symmetry and the presence of intrinsic conduction due to partial band occupation [1–5]. They are rare in solids because free carriers can screen electrostatic potential and eliminate internal dipoles that arise from asymmetric charge distributions [6–10]. Anderson and Blount predicted in 1965 that polar metals can exist [11], and the recent experimental confirmation of  $\text{LiOsO}_3$  as the first polar metal has stimulated intensive theoretical and experimental research [12–21].

However, the above definition of a polar metal (absence of inversion symmetry and presence of conduction) excludes degenerately doped insulating ferroelectrics [21]. Electron doped perovskite ferroelectric compounds  $ABO_3$  ( $\text{BaTiO}_3$  as the prototype) have been widely studied both in theory and in experiment [22–28]. First-principles calculations show that cation displacements and conduction can coexist in  $n$ -doped  $\text{BaTiO}_3$  up to a critical concentration of  $0.1e$  per formula [26]. This indicates that even with long-range Coulomb interaction screened by free electrons [29–31], a short-range portion of Coulomb force with an interaction range of the order of the lattice constant is sufficient to induce ferroelectric instability in  $\text{BaTiO}_3$  [26, 32, 33]. Experimentally, there are contradictory results: Ref. [23, 24] show that in oxygen-reduced  $\text{BaTiO}_{3-\delta}$ , polar displacements can co-exist with conduction and do not vanish until a critical concentration of  $1.9 \times 10^{21} \text{ cm}^{-3}$ , which is consistent with first-principles calculations [26]. However, a neutron diffraction study on  $n$ -doped  $\text{BaTiO}_3$  found phase separation in which ferroelectric displacements only exist in an insulating region, which is spatially separated by nonpolar metallic regions [22]. On the other hand, while electron-doped  $\text{LiNbO}_3$ -type ferroelectric oxides ( $\text{LiNbO}_3$  as the prototype) have been investigated in the literature, the focus has been on electronic structure and the optical property [34–37]. The structural property and the possible co-existence of polar displacements with conduction have received little attention.

In this work, we use first-principles calculations to do a comparative study on doping effects in insulating ferroelectrics. We compare the aforementioned two important classes of ferroelectrics: one is perovskite oxides ( $\text{BaTiO}_3$  as the prototype) and the other is  $\text{LiNbO}_3$ -type oxides ( $\text{LiNbO}_3$  as the prototype). We find different behaviors in these two materials upon electron doping. In the rigid-band approximation, cation displacements in  $n$ -doped  $\text{BaTiO}_3$  quickly get suppressed and completely disappear at a critical doping of  $0.1 e/\text{f.u.}$ ,

while substantial cation displacements are found in  $n$ -doped  $\text{LiNbO}_3$  up to an electron concentration of  $0.3 \text{ e/f.u.}$ . Moreover, Li-O displacements decay more slowly than Nb-O displacements. With an electron doping of  $0.3 \text{ e/f.u.}$ , Nb-O displacements are reduced by about 50% from the undoped value, while Li-O displacements are reduced by only about 10%. This is different from  $n$ -doped  $\text{BaTiO}_3$  in which both Ba-O and Ti-O displacements decay approximately at the same rate. This indicates that Li-O displacements are more persistent than Nb-O displacements in a metallic environment. Supercell calculations that use oxygen vacancy as electron donors support the main results from the rigid-band approximation and provide more detailed charge distributions. We find that in  $n$ -doped  $\text{LiNbO}_3$ , conduction electrons are not as uniformly distributed as in  $n$ -doped  $\text{BaTiO}_3$ , but substantial cation displacements are found throughout  $n$ -doped  $\text{LiNbO}_3$ . Using supercell calculations, we also compute the formation energy of oxygen vacancies. The formation energy of oxygen vacancies in  $n$ -doped  $\text{LiNbO}_3$  is about 1 eV higher than that in  $n$ -doped  $\text{BaTiO}_3$ , which is reasonable considering the fact that the band gap of  $\text{LiNbO}_3$  is about 1 eV larger than that of  $\text{BaTiO}_3$ .

The paper is organized as follows. In Section II we provide computation details. We present the main results (rigid-band calculations and supercell calculations) in Section III. We conclude in Section IV.

## II. COMPUTATIONAL DETAILS

We perform density functional (DFT) calculations [38, 39], as implemented in the Vienna Ab-initio Simulation Package (VASP) [40, 41]. We employ a local density approximation (LDA) pseudopotential [42]. We also test our key results using a revised Perdew-Burke-Ernzerhof generalized gradient approximation (PBEsol) [43]. The key results do not qualitatively change with different exchange correlation functionals. We set an energy cutoff of 600 eV. Charge self-consistent calculations are converged to  $10^{-5} \text{ eV}$ . Both cell and internal coordinates are fully relaxed until each force component is smaller than  $10 \text{ meV/\AA}$  and the stress tensor is smaller than 1 kbar.

For pristine bulk calculations, we use a tetragonal cell (5-atom) to study  $\text{BaTiO}_3$  and find that  $a = 3.95 \text{ \AA}$  and  $c/a = 1.01$ ; we use a hexagonal cell (30-atom) to study  $R3c$   $\text{LiNbO}_3$  and find that  $a = 5.09 \text{ \AA}$  and  $c = 13.81 \text{ \AA}$ . Both of them are in good agreement with previous

studies [44].

To simulate doping effects, we use both the rigid-band approximation and supercell calculations. In rigid-band modeling, we study a 5-atom cell  $\text{BaTiO}_3$  (tetragonal  $P4mm$  and cubic  $Pm\bar{3}m$ ) and a 30-atom cell  $\text{LiNbO}_3$  (non-centrosymmetric  $R3c$  and centrosymmetric  $R\bar{3}c$ ). We use a Monkhorst-Pack  $k$ -point sampling of  $14 \times 14 \times 14$  for  $\text{BaTiO}_3$  and  $8 \times 8 \times 3$  for  $\text{LiNbO}_3$ . In supercell calculations, we use a 119-atom cell for both  $\text{BaTiO}_3$  and  $\text{LiNbO}_3$  (oxygen vacancy concentration of 4.2%/f.u. and nominally electron doping of 0.084  $e$ /f.u.). The supercells for  $\text{BaTiO}_3$  and  $\text{LiNbO}_3$  are shown in Fig. 4 and Fig. 5. We use a Monkhorst-Pack  $k$ -point sampling of  $8 \times 8 \times 8$  in supercell calculations.

In our supercell calculations, we remove one (charge neutral) oxygen atom in  $\text{LiNbO}_3$  supercells of different sizes to simulate different oxygen vacancy concentrations. The supercell with oxygen vacancies is charge-neutral, and we fully relax the structure (both lattice constants and internal coordinates) to get the ground state property.

We check a higher energy cutoff (750 eV) and a denser  $k$ -point sampling, and we do not find any significant changes in the key results.

### III. RESULTS AND DISCUSSION

#### A. Rigid-band calculations

In the rigid-band approximation, materials are pristine and extra electrons are added to the system with the same amount of uniform positive charges in the background. Fig. 1 shows the crystal structures of pristine  $\text{BaTiO}_3$  and  $\text{LiNbO}_3$ , which are used in rigid-band modeling. Panels **a1** and **a2** show the crystal structure of cubic  $\text{BaTiO}_3$  (space group  $Pm\bar{3}m$ ) and tetragonal  $\text{BaTiO}_3$  (space group  $P4mm$ ). Insulating ferroelectrics have a spontaneous polarization [45]. However, in doped ferroelectrics, partially filled bands may lead to conduction and polarization becomes ill-defined [46–48]. Therefore, we use cation displacements to characterize the extent of being “polar”. In  $n$ -doped  $\text{BaTiO}_3$ , we calculate both Ba-O and Ti-O cation displacements along the  $c$ -axis, denoted by  $\delta_{\text{Ba-O}}$  and  $\delta_{\text{Ti-O}}$ , as a function of electron concentration.  $\delta_{\text{Ba-O}}$  and  $\delta_{\text{Ti-O}}$  are explicitly shown in Fig. S1 in the Supplementary Materials. Panels **b1** and **b2** show the crystal structure of centrosymmetric  $\text{LiNbO}_3$  (space group  $R\bar{3}c$ ) and non-centrosymmetric  $\text{LiNbO}_3$  (space group  $R3c$ ). We calculate both

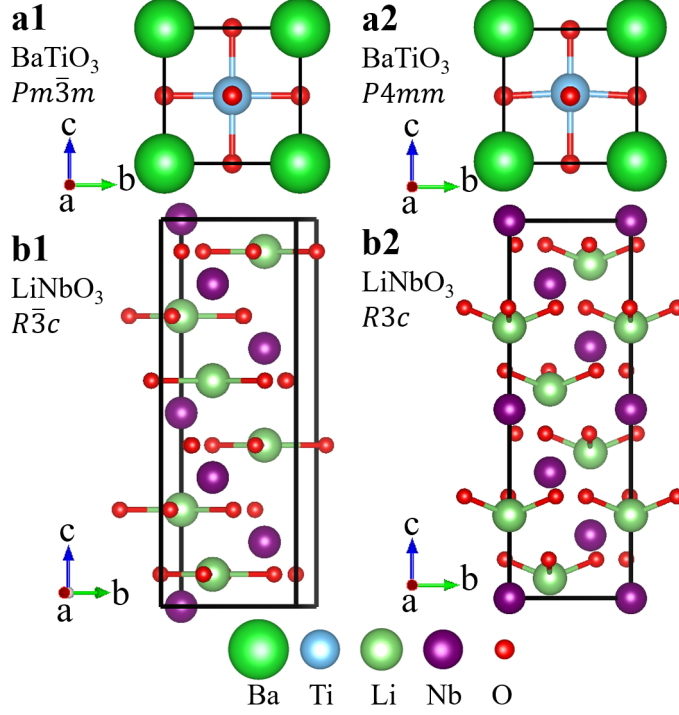


FIG. 1. Atomic structures of  $\text{BaTiO}_3$  and  $\text{LiNbO}_3$ . Panels **a1**) and **a2**) show cubic  $Pm\bar{3}m$  and tetragonal  $P4mm$  structures of  $\text{BaTiO}_3$ , respectively. Panels **b1**) and **b2**) show centrosymmetric  $R\bar{3}c$  and non-centrosymmetric  $R3c$  structures of  $\text{LiNbO}_3$ , respectively.

Li-O and Nb-O displacements  $\delta_{\text{Li-O}}$  and  $\delta_{\text{Nb-O}}$ . In the centrosymmetric structure  $R\bar{3}c$ , each Li atom is surrounded by three oxygen atoms and all these four atoms form a plane that is perpendicular to  $c$ -axis. In the non-centrosymmetric structure  $R3c$ , the three oxygen atoms still form a plane that is perpendicular to the  $c$ -axis but Li atom deviates from that plane. The distance between Li atom and the plane that the three oxygen atoms form is defined as the Li-O displacement  $\delta_{\text{Li-O}}$ . In the centrosymmetric structure  $R\bar{3}c$ , each Nb atom is at the center of an  $\text{NbO}_6$  oxygen octahedron. In the non-centrosymmetric structure  $R3c$ , Nb atoms move off the center of the  $\text{NbO}_6$  oxygen octahedron. The distance between the Nb position and the center of the oxygen octahedron in the  $R3c$  structure is defined as  $\delta_{\text{Nb-O}}$ .  $\delta_{\text{Li-O}}$  and  $\delta_{\text{Nb-O}}$  are explicitly shown in Fig. S2 in the Supplementary Materials.

Fig. 2 summarizes the key results from rigid-band calculations. Panel **a** shows the cation displacements of tetragonal  $\text{BaTiO}_3$  (space group  $P4mm$ ) and non-centrosymmetric  $\text{LiNbO}_3$  (space group  $R3c$ ). In the undoped case,  $\delta_{\text{Ba-O}} = 0.077 \text{ \AA}$  and  $\delta_{\text{Ti-O}} = 0.099 \text{ \AA}$  in  $\text{BaTiO}_3$ , and  $\delta_{\text{Li-O}} = 0.723 \text{ \AA}$  and  $\delta_{\text{Nb-O}} = 0.261 \text{ \AA}$  in  $\text{LiNbO}_3$ , both of which are in good agree-

ment with previous calculations and experiments [7, 49–51]. Upon doping, all of the cation displacements decrease with increasing electron concentration.  $\delta_{\text{Ba-O}}$  and  $\delta_{\text{Ti-O}}$  in  $n$ -doped  $\text{BaTiO}_3$  vanish at  $n_c \simeq 0.1$   $e/\text{f.u.}$ , which is consistent with previous calculations [26]. However,  $\delta_{\text{Li-O}}$  and  $\delta_{\text{Nb-O}}$  in  $n$ -doped  $\text{LiNbO}_3$  persist up to 0.3  $e/\text{f.u.}$ . Furthermore, in  $n$ -doped  $\text{BaTiO}_3$ ,  $\delta_{\text{Ba-O}}$  and  $\delta_{\text{Ti-O}}$  decay at approximately the same rate. But in  $n$ -doped  $\text{LiNbO}_3$ ,  $\delta_{\text{Li-O}}$  decays more slowly than  $\delta_{\text{Nb-O}}$ . With 0.3  $e/\text{f.u.}$  electron doping, Nb-O displacements are reduced by about 50% from the undoped value, while Li-O displacements are reduced by only about 10%. This indicates that the off-center movements of Li atoms are very robust and more persistent than Nb-O displacements in a metallic environment. This helps to create an approximate polar metallic phase when  $\text{LiNbO}_3$  is electron doped.

Panel **b** of Fig. 2 shows the energy difference between the centrosymmetric structure and the non-centrosymmetric structure of  $\text{BaTiO}_3$  and  $\text{LiNbO}_3$ . Specifically, for  $\text{BaTiO}_3$   $\Delta E = E(Pm\bar{3}m) - E(P4mm)$  and for  $\text{LiNbO}_3$   $\Delta E = E(R\bar{3}c) - E(R3c)$ .  $\Delta E > 0$  indicates that the non-centrosymmetric structure is favored. In the undoped case, the non-centrosymmetric structure is favored in both  $\text{BaTiO}_3$  and  $\text{LiNbO}_3$ , i.e. they are both ferroelectric. Upon doping,  $\text{BaTiO}_3$  is polar till  $n_c \simeq 0.1$   $e/\text{f.u.}$ , consistent with the critical concentration found for  $\delta_{\text{Ba-O}}$  and  $\delta_{\text{Ti-O}}$ . For  $n$ -doped  $\text{LiNbO}_3$ ,  $\Delta E$  quickly decreases but it stays positive (up to 0.3  $e/\text{f.u.}$ ). This is consistent with  $\delta_{\text{Li-O}}$  and  $\delta_{\text{Nb-O}}$ , which do not vanish with electron doping (up to 0.3  $e/\text{f.u.}$ ).

Panel **c** of Fig. 2 shows the zone-center phonon frequency of the ferroelectric mode for centrosymmetric  $\text{BaTiO}_3$  (space group  $Pm\bar{3}m$ ) and  $\text{LiNbO}_3$  (space group  $R\bar{3}c$ ). For cubic  $Pm\bar{3}m$   $\text{BaTiO}_3$ , the ferroelectric mode has imaginary phonon frequency with small electron doping, indicating ferroelectric instability. Around the critical doping of  $n_c \simeq 0.1$   $e/\text{f.u.}$  the phonon frequency of the ferroelectric mode becomes positive and the cubic structure is stabilized. For centrosymmetric  $R\bar{3}c$   $\text{LiNbO}_3$ , the ferroelectric mode always has imaginary phonon frequency (up to 0.3  $e/\text{f.u.}$ ), indicating that ferroelectric instability persists in  $n$ -doped  $\text{LiNbO}_3$ . For both materials, the phonon property of the centrosymmetric structures is consistent with the results of the non-centrosymmetric structures shown in panels **a** and **b**. We note that the magnitude of the imaginary phonon mode indicates how unstable the high-symmetry structure is subject to a collective atomic distortion. However, the energy difference between the distorted and undistorted crystal structures reflects not only the instability of the high-symmetry structure, but also other factors. From our calculations,

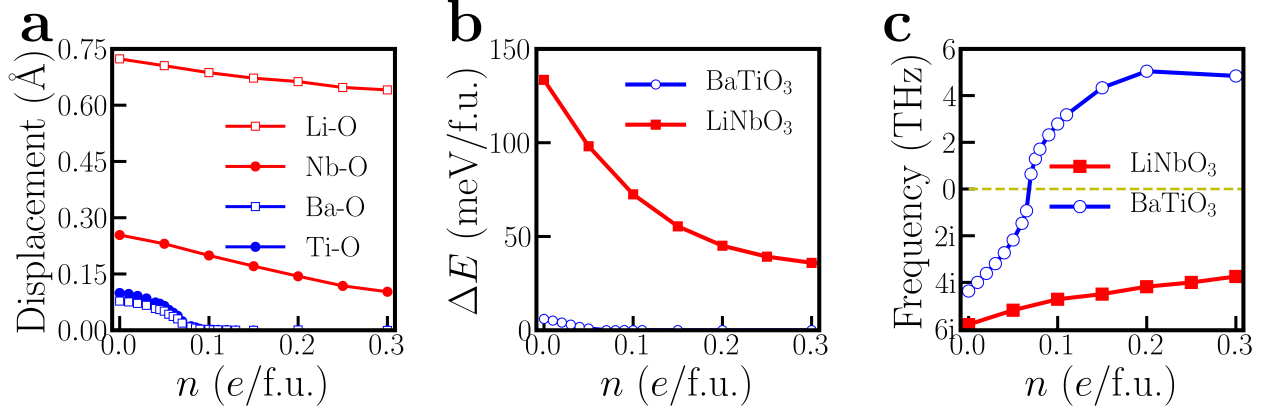


FIG. 2. Panel **a**) Ba-O, Ti-O, Li-O and Nb-O displacements in non-centrosymmetric structures of BaTiO<sub>3</sub> and LiNbO<sub>3</sub> as a function of electron doping. Panel **b**) energy difference between the centrosymmetric and the non-centrosymmetric structures of BaTiO<sub>3</sub> and LiNbO<sub>3</sub> as a function of electron doping. Panel **c**) phonon frequency of the zone-center ferroelectric mode of cubic BaTiO<sub>3</sub> and  $R\bar{3}c$  LiNbO<sub>3</sub> as a function of electron doping.

we find that for BaTiO<sub>3</sub>, the volume of its undistorted structure is 0.5% smaller than that of the distorted structure; in contrast, for LiNbO<sub>3</sub>, the volume of its undistorted structure is 1.5% larger than that of the distorted structure. The elastic energy change from the high-symmetry structure to the low-symmetry structure is very different between BaTiO<sub>3</sub> and LiNbO<sub>3</sub>. This information is embodied in the total energy difference but is not directly reflected in the imaginary phonon modes.

We also use the PBEsol functional to check the key results in Fig. 2, and we do not find significant changes (see Fig. S4 in the Supplementary Materials). Our finding that polar displacements of LiNbO<sub>3</sub> are persistent in the presence of conduction electrons is related to the fact that LiNbO<sub>3</sub> is hyperferroelectric [52, 53], i.e. a ferroelectric material whose polarization does not get suppressed by depolarization fields. This implies that doping a hyperferroelectric material is a viable approach to generating an approximate polar metallic phase.

Next, we study the electronic structure and screening length obtained from rigid-band calculations. Panels **a1** and **a2** of Fig. 3 show the density of states of undoped and doped BaTiO<sub>3</sub> (with 0.2  $e/f.u.$  doping). With electron doping, the Fermi level is shifted from the band gap into Ti- $d$  states. Panels **b1** and **b2** of Fig. 3 show the density of states of undoped



and doped LiNbO<sub>3</sub> (with 0.2  $e/f.u.$  doping). Similarly, with electron doping, the Fermi level is shifted from the band gap into Nb- $d$  states. With the density of states of  $n$ -doped BaTiO<sub>3</sub> and  $n$ -doped LiNbO<sub>3</sub>, we can estimate the screening length  $\lambda$  by using the Thomas-Fermi model [26]:

$$\lambda = \sqrt{\frac{\epsilon}{e^2 \times D(E_f)}} \quad (1)$$

where  $\epsilon$  is the dielectric constant of undoped materials and  $D(E_f)$  is density of states at Fermi level. For dielectric constants, we use experimental values  $\epsilon \approx 44\epsilon_0$  for BaTiO<sub>3</sub> [54] and  $\epsilon \approx 24\epsilon_0$  for LiNbO<sub>3</sub> [55]. Panels **c** of Fig. 3 show the screening length of  $n$ -doped BaTiO<sub>3</sub> and  $n$ -doped LiNbO<sub>3</sub>. We find that for both materials upon electron doping, the screening length is on the order of a few Å. Given an electron concentration,  $n$ -doped LiNbO<sub>3</sub> even has a screening length slightly smaller than  $n$ -doped BaTiO<sub>3</sub>, implying a stronger screening property. The stronger screening property of electron doped LiNbO<sub>3</sub> is due to the fact that undoped LiNbO<sub>3</sub> has a smaller dielectric constant than that of BaTiO<sub>3</sub>, while the density of states at the Fermi level plays a minor role (the ratio of  $D(E_f)_{\text{LiNbO}_3}$  to  $D(E_f)_{\text{BaTiO}_3}$  ranges from 0.9 to 1.1 as  $n$  changes from 0 to 0.3  $e/f.u.$ ).

## B. Supercell calculations

Our rigid-band calculations show that polar displacements and conduction can coexist in both  $n$ -doped BaTiO<sub>3</sub> and  $n$ -doped LiNbO<sub>3</sub>, but the overall polar property (magnitude of polar displacements, polar instability, etc.) is much more enhanced in  $n$ -doped LiNbO<sub>3</sub> than in  $n$ -doped BaTiO<sub>3</sub>. However, rigid-band calculations do not specify the origin of electron doping and also they imply that all carriers are uniformly distributed. In real experiments, oxygen vacancies are commonly seen in complex oxides, and each oxygen vacancy nominally donates two electrons. However, an isolated oxygen vacancy may form a defect state, which can localize conduction electrons [56, 57]. Some experiments shows that in oxygen-reduced BaTiO<sub>3- $\delta$</sub> , phase separation occurs. Cation displacements  $\delta_{\text{Ti-O}}$  only occur in the insulating region and vanish in the metallic region. The overall sample may be considered as a mixture of two different phases [22]. To test whether the results from the rigid-band calculations remain valid in real materials, we perform supercell calculations and consider charge neutral oxygen vacancies as the electron doping source. We use a 119-atom cell of BaTiO<sub>3- $\delta$</sub>  and

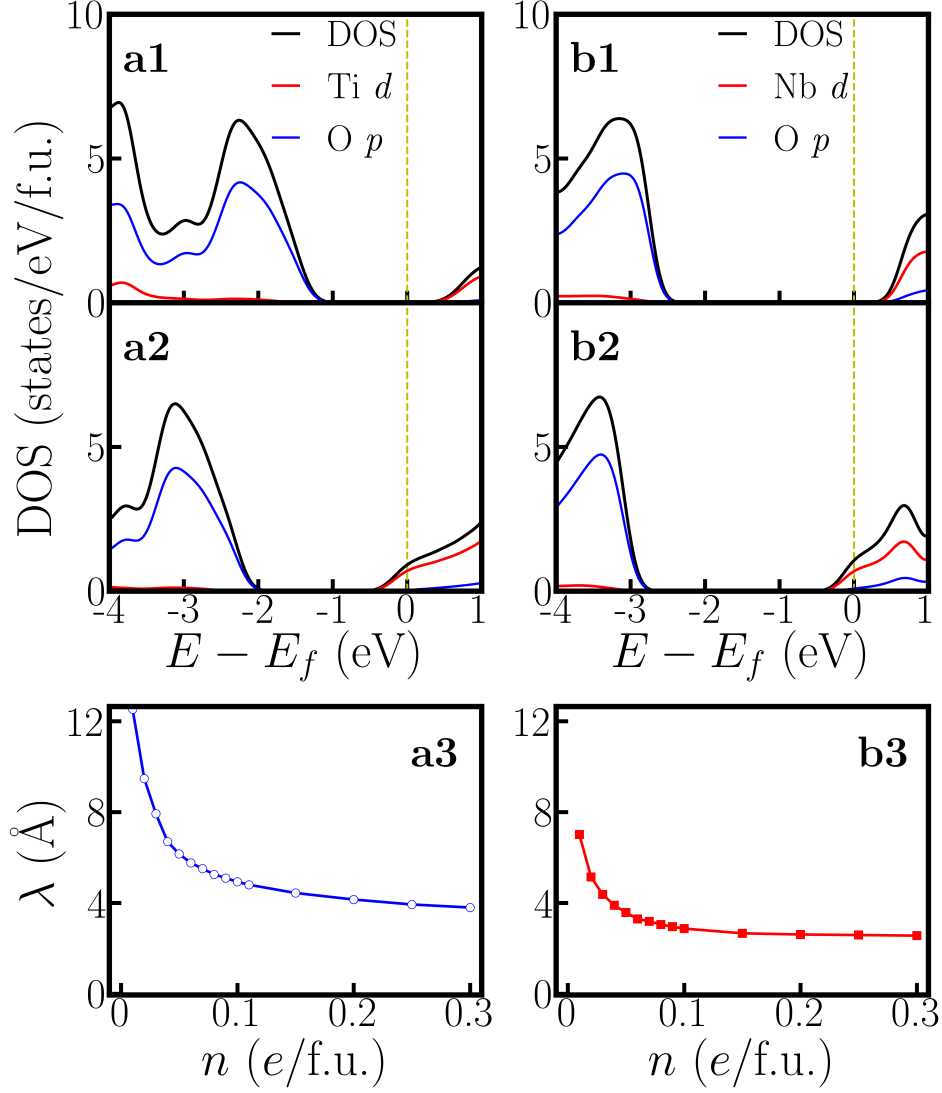


FIG. 3. Panel **a1**) density of states of undoped BaTiO<sub>3</sub>. Panel **a2**) density of states of doped BaTiO<sub>3</sub> with 0.2 *e*/f.u. doping. The black, red and blue are total, Ti-*d* and O-*p* projected densities of states, respectively. Panel **b1**) density of states of undoped LiNbO<sub>3</sub>. Panel **b2**) density of states of doped LiNbO<sub>3</sub> with 0.2 *e*/f.u. doping. The black, red and blue are total, Nb-*d* and O-*p* projected densities of states respectively. Panel **a3**) Thomas-Fermi screening length  $\lambda$  of doped BaTiO<sub>3</sub> as a function of electron doping *n*. Panel **b3**) Thomas-Fermi screening length  $\lambda$  of doped LiNbO<sub>3</sub> as a function of electron doping *n*.

LiNbO<sub>3- $\delta$</sub> . In both cases, the oxygen vacancy concentration is 4.2%/f.u.. A charge neutral oxygen vacancy donates two electrons to the system, therefore it is an electron doping of 0.084 *e*/f.u. ( $\simeq 1.5 \times 10^{21}$  cm<sup>-3</sup>), close to the critical doping in *n*-doped BaTiO<sub>3</sub> obtained

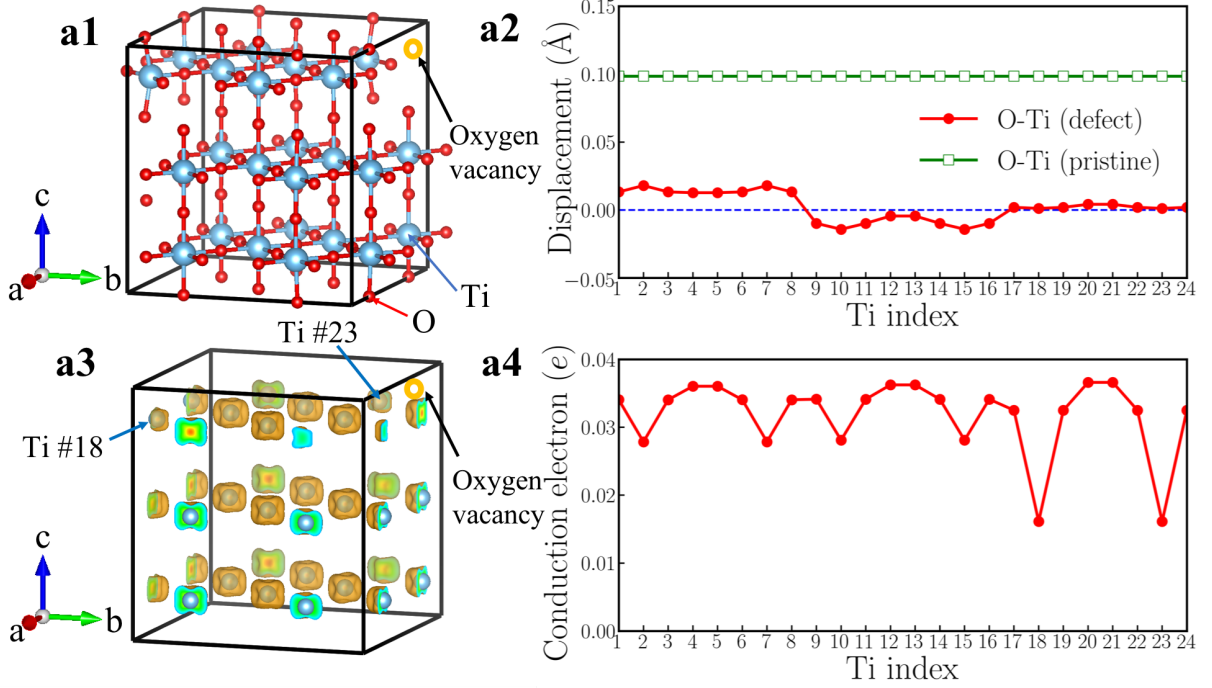


FIG. 4. Panel **a1**) atomic structure of 119-atom  $\text{BaTiO}_{3-\delta}$  supercell that contains an oxygen vacancy. For clarity, Ba atoms are not shown. The blue and red balls represent Ti and O atoms. Panel **a2**) polar displacements of each Ti atom. The red circles are calculated from the 119-atom cell. The green squares are bulk  $\delta_{\text{Ti-O}}$  of pristine  $\text{BaTiO}_3$ . Panel **a3**) an iso-value surface of conduction electron distribution in oxygen-reduced  $\text{BaTiO}_{3-\delta}$  with  $\delta = 4.2\%$ . The two nearest neighbor Ti atoms are highlighted. Panel **a4**) conduction electrons on each Ti atom in the 119-atom cell (the number of conduction electron on each Ti atom is obtained by integrating Ti-*d* states from band gap to the Fermi level).

from rigid-band calculations.

Fig. 4**a1** shows the crystal structure of a 119-atom  $\text{BaTiO}_{3-\delta}$  supercell that contains one oxygen vacancy. For clarity, Ba atoms are not explicitly shown and the oxygen vacancy is highlighted by the orange open circle. Fig. 4**a2** shows the cation displacement  $\delta_{\text{Ti-O}}$  for each Ti atom in the  $\text{BaTiO}_{3-\delta}$  supercell (the definition of  $\delta_{\text{Ti-O}}$  is identical to that in the rigid-band calculations). Displacements along *c*-axis of each Ba atom are explicitly shown in Fig. S3 in the Supplementary Materials. We find that while there is some small variation in  $\delta_{\text{Ti-O}}$  due to an inhomogeneous chemical environment,  $\delta_{\text{Ti-O}}$  on average is reduced to zero. For comparison, we also show the  $\delta_{\text{Ti-O}}$  in pristine  $\text{BaTiO}_3$  in panel **a2** and the

suppression of polar displacements by electron doping is evident. Fig. 4a3 shows an iso-value surface of conduction electron density in oxygen-reduced  $\text{BaTiO}_{3-\delta}$  with  $\delta = 4.2\%$ . Conduction electrons reside on Ti atoms. Because the polar displacements are suppressed and the material is close to a cubic structure, conduction electrons occupy three Ti  $t_{2g}$  orbitals with approximately equal occupancy. This leads to an iso-value surface of a dice-like shape. Fig. 4a4 shows the number of conduction electrons on each Ti atom by integrating the Ti- $d$  states from the band gap to the Fermi level. We find that in the presence of oxygen vacancy, while there is non-negligible variation in conduction electron distribution, insulating-metallic phase separation does not occur in our first-principles calculations. Each Ti atom in the supercell has a sizable amount of conduction electron. The results of oxygen-reduced  $\text{BaTiO}_{3-\delta}$  from supercell calculations are very consistent with rigid-band calculations. We also use the LDA+ $U$  method and change the supercell size to test the robustness of this conclusion (see the Supplementary Materials for details). We find that in oxygen-reduced  $\text{BaTiO}_{3-\delta}$ , conduction electrons on each Ti atom are almost uniformly distributed.

However, supercell calculations of oxygen-reduced  $\text{LiNbO}_{3-\delta}$  show more complicated results than rigid-band calculations. Fig. 5a1 shows the crystal structure of a 119-atom  $\text{LiNbO}_3$  supercell that contains one oxygen vacancy. The oxygen vacancy is highlighted by the orange open circle. Fig. 5a2 shows  $\delta_{\text{Li-O}}$  for each Li atom and  $\delta_{\text{Nb-O}}$  for each Nb atom in the  $\text{LiNbO}_{3-\delta}$  supercell (the definitions of  $\delta_{\text{Li-O}}$  and  $\delta_{\text{Nb-O}}$  are identical to those in the rigid-band calculations). We find that while there is non-negligible variation in  $\delta_{\text{Li-O}}$  and  $\delta_{\text{Nb-O}}$ , the cation displacements on each Li and Nb atoms are non-zero throughout the supercell. For comparison, we also show the  $\delta_{\text{Li-O}}$  and  $\delta_{\text{Nb-O}}$  in pristine  $\text{LiNbO}_3$  in panel a2. We find that in the presence of oxygen vacancy in  $\text{LiNbO}_{3-\delta}$ , the cation displacements are still substantial, compared to undoped  $\text{LiNbO}_3$ .

The average value of  $\delta_{\text{Li-O}}$  is 0.68 Å and the average value of  $\delta_{\text{Nb-O}}$  is 0.24 Å, both of which are close to the results of rigid-band calculations with the same electron concentration (in the rigid-band approximation,  $\delta_{\text{Li-O}}$  is 0.69 Å and  $\delta_{\text{Nb-O}}$  is 0.21 Å). Fig. 5a3 shows an iso-value surface of conduction electron distribution in oxygen-reduced  $\text{LiNbO}_{3-\delta}$  with  $\delta = 4.2\%$ . Different from oxygen-reduced  $\text{BaTiO}_{3-\delta}$  which has almost uniform conduction electron distribution, some of Nb atoms have negligible conduction electrons, indicating that those Nb sites are almost insulating. This phenomenon can be more clearly seen from Fig. 5a4,

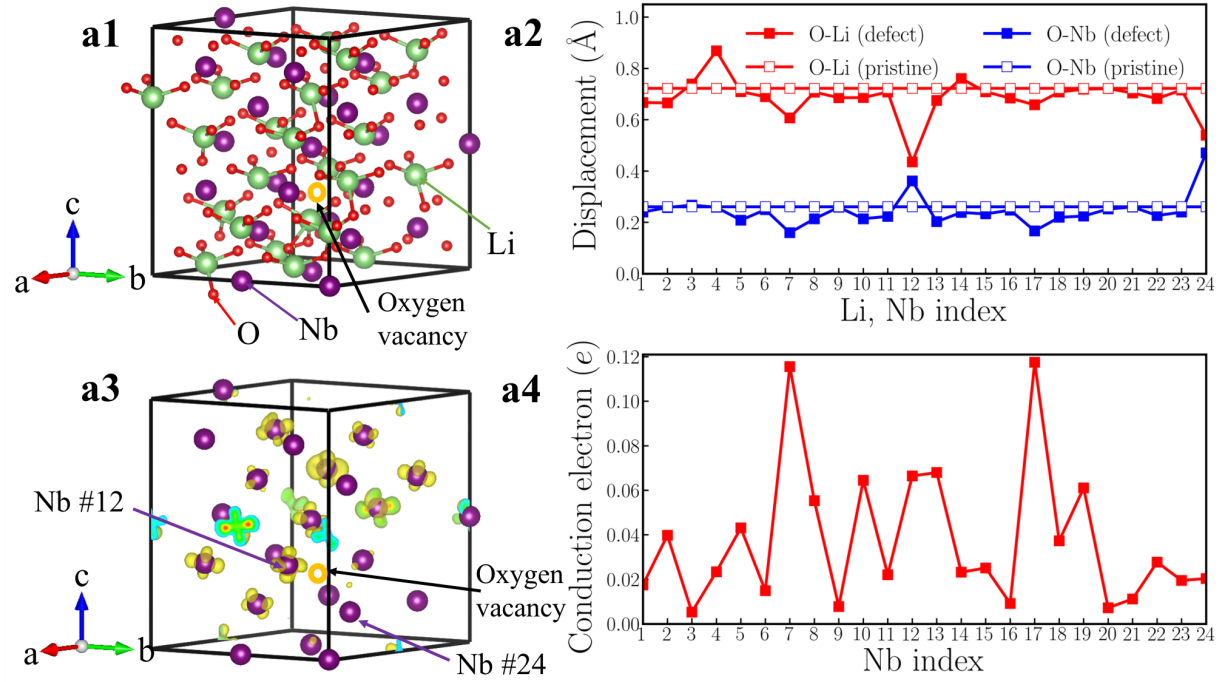


FIG. 5. Panel **a1**) atomic structure of 119-atom  $\text{LiNbO}_3$  supercell that contains an oxygen vacancy. The green, purple and red balls represent Li, Nb and O atoms respectively. The orange circle highlights an oxygen vacancy. Panel **a2**) polar displacements of each Li (red square) and Nb atom (blue square). The solid squares are calculated from the 119-atom cell. The open squares are bulk  $\delta_{\text{Li-O}}$  and  $\delta_{\text{Nb-O}}$  of pristine  $\text{LiNbO}_3$ . Panel **a3**) an iso-value surface of conduction electron distribution in oxygen-reduced  $\text{LiNbO}_{3-\delta}$  with  $\delta = 4.2\%$ . The two nearest neighbor Nb atoms are highlighted. Panel **a4**) conduction electrons on each Nb atom in the 119-atom cell (the number of conduction electron on each Nb atom is obtained by integrating Nb- $d$  states from band gap to the Fermi level).

which shows the number of conduction electrons on each Nb site by integrating Nb- $d$  states from the band gap to the Fermi level. Nb #3, #9 and #20 have less than 0.01  $e$  per atom, while Nb #7 and #17 have more than 0.12  $e$  per atom. With electron doping in  $\text{LiNbO}_3$ , the conduction electrons on Nb sites are far from uniformly distributed. This implies that the charge disproportionation of conduction electrons on Nb atoms occurs in real materials. Such charge disproportionation can be suppressed with a higher electron concentration. We calculated oxygen-reduced  $\text{LiNbO}_{3-\delta}$  with  $\delta = 8.4\%$ . Cation displacements and conduction electron distribution on Nb- $d$  states are shown in Fig. S9 in the Supplementary Materials. While

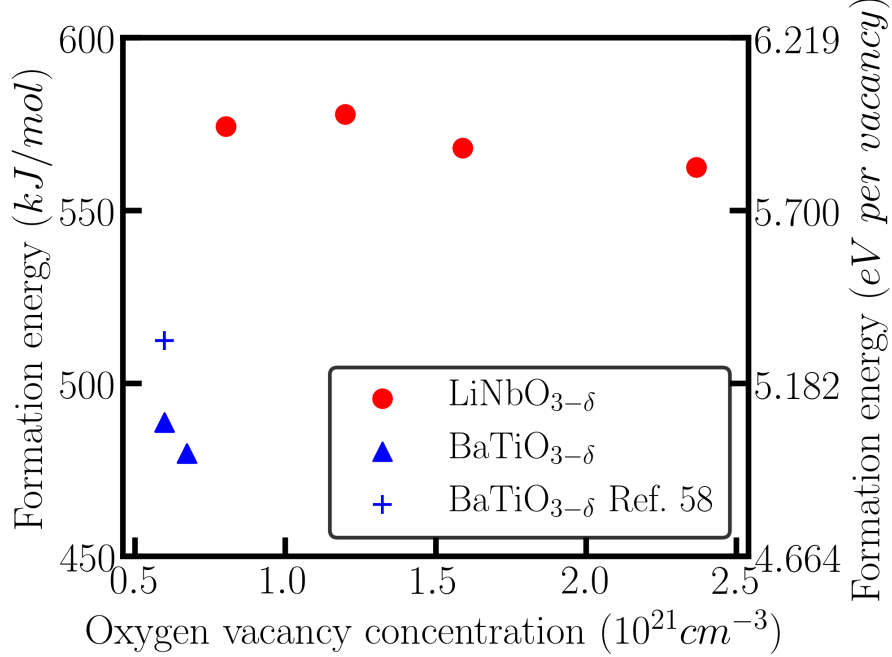


FIG. 6. Oxygen vacancy formation energy in oxygen-reduced BaTiO<sub>3-δ</sub> (blue triangles) and in oxygen-reduced LiNbO<sub>3-δ</sub> (red circles) as a function of oxygen vacancy concentration. The blue cross is a reference value from previous works [58].

there is non-negligible variation in the electron distribution, all Nb atoms have conduction electrons with a higher concentration of oxygen vacancies, as expected.

Finally we estimate the formation energy of a charge-neutral oxygen vacancy in BaTiO<sub>3-δ</sub> and in LiNbO<sub>3-δ</sub> using a supercell calculation. We study a charge neutral oxygen vacancy by removing an oxygen atom from a charge neutral supercell. The definition of formation energy of a charge-neutral oxygen vacancy in the oxygen rich limit is:

$$\Delta E_O^f = E_T(V_O) - E_{T0} + \frac{1}{2}E_{O_2} \quad (2)$$

where  $E_T(V_O)$  is the total energy of a supercell with one oxygen vacancy, and  $E_{T0}$  is the total energy of a pristine supercell.  $E_{O_2}$  is the total energy of an oxygen molecule (obtained in a spin-polarized calculation).

Fig. 6 shows the oxygen vacancy formation energy in oxygen-reduced BaTiO<sub>3-δ</sub> and oxygen-reduced LiNbO<sub>3-δ</sub> as a function of oxygen vacancy concentration. Red points and blue triangles are the formation energies of oxygen vacancy in BaTiO<sub>3-δ</sub> and LiNbO<sub>3-δ</sub>, respectively. The blue cross is a reference value from previous works [58].

We use different supercells to test different concentrations of oxygen vacancies. The formation energy of an oxygen vacancy does not have a strong dependence on vacancy concentration, implying that the vacancy concentration is low enough such that vacancy-vacancy interaction is negligible. The formation energy of a charge neutral oxygen vacancy in  $\text{LiNbO}_{3-\delta}$  is larger than that in  $\text{BaTiO}_{3-\delta}$  by about 0.9 eV per vacancy. This is reasonable considering the fact that the gap of  $\text{LiNbO}_3$  is larger than that of  $\text{BaTiO}_3$  by about 1 eV (see Fig. 3). While the formation energy of oxygen vacancy in  $\text{LiNbO}_{3-\delta}$  is higher, oxygen vacancy has been widely observed in  $\text{LiNbO}_{3-\delta}$  in experiments [59–62].

#### IV. CONCLUSION

In conclusion, we perform first-principles calculations to study the possible co-existence of conduction electrons and polar distortions in  $n$ -doped  $\text{BaTiO}_3$  and  $n$ -doped  $\text{LiNbO}_3$ , using both rigid-band modeling and more realistic supercell calculations. From rigid-band modeling, we find that upon electron doping, cation displacements in  $\text{BaTiO}_3$  are quickly reduced and completely vanish at a critical electron concentration of 0.1  $e/\text{f.u.}$ . In contrast, in  $n$ -doped  $\text{LiNbO}_3$ , Li-O and Nb-O displacements are significantly larger than cation displacements in  $n$ -doped  $\text{BaTiO}_3$ , and more importantly they are much more robust and can persist even at a concentration of 0.3  $e/\text{f.u.}$ . In  $n$ -doped  $\text{LiNbO}_3$ , Li-O displacements decay more slowly than Nb-O displacements, while in  $n$ -doped  $\text{BaTiO}_3$ , Ba-O and Ti-O displacements decay approximately at the same rate. From supercell calculations (using oxygen vacancy as electron donors), we find that in  $\text{BaTiO}_{3-\delta}$  with  $\delta = 4.2\%$ , cation displacements in  $\text{BaTiO}_3$  are almost completely suppressed, which is consistent with the result of rigid-band modeling. Conduction electrons on Ti atoms are uniformly distributed, underlying rigid-band calculations. On the other hand, the results of oxygen-reduced  $\text{LiNbO}_{3-\delta}$  ( $\delta = 4.2\%$ ) from supercell calculations are more complicated than rigid-band calculations. Substantial polar displacements  $\delta_{\text{Li-O}}$  and  $\delta_{\text{Nb-O}}$  occur throughout the supercell, but strong variations are found in conduction electron distribution. This implies that the rigid-band approximation should be used with caution in simulating electron doped  $\text{LiNbO}_3$  and related oxides.

Our work indicates that electron doping of  $\text{LiNbO}_3$ -type ferroelectrics is a simple and feasible approach to approximately creating the rare polar metallic phase. Incorporating

doped ferroelectric semiconductors (in particular  $\text{LiNbO}_3$ -type ferroelectrics) into devices may lead to new functionality and applications.

## ACKNOWLEDGMENTS

Hanghui Chen is supported by the National Natural Science Foundation of China under project number 11774236, Shanghai Pujiang Talents Program (Grant No. 17PJ1407300) and Seed grant of NYU-ECNU Research Institute of Physics. Yue Chen and Chengliang Xia are supported by Research Grants Council of Hong Kong under project numbers 17200017 and 17300018, and the National Natural Science Foundation of China under project number 11874313. NYU Shanghai HPC and HKU-ITS provide computational resources.

---

\* Correspondence to hanghui.chen@nyu.edu or yuechen@hku.hk.

- [1] D. Puggioni and J. M. Rondinelli, *Nature Communications* **5**, 3432 (2014).
- [2] Y. Cao, Z. Wang, S. Y. Park, Y. Yuan, X. Liu, S. M. Nikitin, H. Akamatsu, M. Kareev, S. Middey, D. Meyers, et al., *Nature Communications* **9**, 1547 (2018).
- [3] P. V. Balachandran, J. Young, T. Lookman, and J. M. Rondinelli, *Nature Communications* **8**, 14282 (2017).
- [4] K. Page, T. Kolodiaznyi, T. Proffen, A. K. Cheetham, and R. Seshadri, *Physical Review Letters* **101**, 205502 (2008).
- [5] J. A. Bock, S. Lee, S. Trolier-McKinstry, and C. A. Randall, *Applied Physics Letters* **107**, 092902 (2015).
- [6] L. S. McCarty and G. M. Whitesides, *Angewandte Chemie International Edition* **47**, 2188 (2008).
- [7] K. M. Rabe, C. H. Ahn, and J.-M. Triscone, *Physics of ferroelectrics: a modern perspective*, vol. 105 (Springer Science & Business Media, 2007).
- [8] A. Mooradian and G. Wright, *Physical Review Letters* **16**, 999 (1966).
- [9] J. Bowlan, Ph.D. thesis, Georgia Institute of Technology (2010).
- [10] N. A. Hill, *Why are there so few magnetic ferroelectrics?* (2000).
- [11] P. W. Anderson and E. Blount, *Physical Review Letters* **14**, 217 (1965).



- [12] Y. Shi, Y. Guo, X. Wang, A. J. Princep, D. Khalyavin, P. Manuel, Y. Michiue, A. Sato, K. Tsuda, S. Yu, et al., *Nature Materials* **12**, 1024 (2013).
- [13] H. Xiang, *Physical Review B* **90**, 094108 (2014).
- [14] G. Giovannetti and M. Capone, *Physical Review B* **90**, 195113 (2014).
- [15] H. Liu, Y. Du, Y. Xie, J.-M. Liu, C.-G. Duan, and X. Wan, *Physical Review B* **91**, 064104 (2015).
- [16] E. I. P. Aulesti, Y. W. Cheung, Y.-W. Fang, J. He, K. Yamaura, K. T. Lai, S. K. Goh, and H. Chen, *Appl. Phys. Lett.* **113**, 12902 (2018).
- [17] I. L. Vecchio, G. Giovannetti, M. Autore, P. Di Pietro, A. Perucchi, J. He, K. Yamaura, M. Capone, and S. Lupi, *Physical Review B* **93**, 161113 (2016).
- [18] H. Sim and B. G. Kim, *Physical Review B* **89**, 201107 (2014).
- [19] H. Padmanabhan, Y. Park, D. Puggioni, Y. Yuan, Y. Cao, L. Gasparov, Y. Shi, J. Chakhalian, J. M. Rondinelli, and V. Gopalan, *Applied Physics Letters* **113**, 122906 (2018).
- [20] Z. Fei, W. Zhao, T. A. Palomaki, B. Sun, M. K. Miller, Z. Zhao, J. Yan, X. Xu, and D. H. Cobden, *Nature* **560**, 336 (2018).
- [21] T. Kim, D. Puggioni, Y. Yuan, L. Xie, H. Zhou, N. Campbell, P. Ryan, Y. Choi, J.-W. Kim, J. Patzner, et al., *Nature* **533**, 68 (2016).
- [22] I.-K. Jeong, S. Lee, S.-Y. Jeong, C. J. Won, N. Hur, and A. Llobet, *Phys. Rev. B* **84**, 064125 (2011).
- [23] J. Hwang, T. Kolodiaznyi, J. Yang, and M. Couillard, *Physical Review B* **82**, 214109 (2010).
- [24] T. Kolodiaznyi, M. Tachibana, H. Kawaji, J. Hwang, and E. Takayama-Muromachi, *Physical Review Letters* **104**, 147602 (2010).
- [25] T. Kolodiaznyi, *Physical Review B* **78**, 045107 (2008).
- [26] Y. Wang, X. Liu, J. D. Burton, S. S. Jaswal, and E. Y. Tsymlal, *Physical Review Letters* **109**, 247601 (2012).
- [27] S. Raghavan, J. Y. Zhang, O. F. Shoron, and S. Stemmer, *Physical Review Letters* **117**, 037602 (2016).
- [28] C. Won, Y. Park, K. Lee, H. Ryu, and N. Hur, *Journal of Applied Physics* **109**, 084108 (2011).
- [29] D. Bohm and D. Pines, *Physical Review* **92**, 609 (1953).
- [30] W. Cochran, *Adv. Phys.* **9**, 387 (1960).
- [31] V. Galitski and S. D. Sarma, *Physical Review B* **70**, 035111 (2004).

- [32] Q. Zhang, T. Cagin, and W. A. Goddard, *Proceedings of the National Academy of Sciences* **103**, 14695 (2006).
- [33] R. E. Cohen, *Nature* **358**, 136 (1992).
- [34] Y. Furukawa, K. Kitamura, A. Alexandrovski, R. Route, M. Fejer, and G. Foulon, *Applied Physics Letters* **78**, 1970 (2001).
- [35] G. Nataf, P. Grysan, M. Guennou, J. Kreisel, D. Martinotti, C. Rountree, C. Mathieu, and N. Barrett, *Scientific Reports* **6**, 33098 (2016).
- [36] K. Nakamura, J. Kurz, K. Parameswaran, and M. Fejer, *Journal of Applied Physics* **91**, 4528 (2002).
- [37] Y. Noguchi, R. Inoue, and M. Miyayama, *Advances in Condensed Matter Physics* **2016** (2016).
- [38] P. Hohenberg and W. Kohn, *Physical Review* **136**, B864 (1964).
- [39] W. Kohn and L. J. Sham, *Physical Review* **140**, A1133 (1965).
- [40] M. C. Payne, M. P. Teter, D. C. Allan, T. Arias, and a. J. Joannopoulos, *Reviews of Modern Physics* **64**, 1045 (1992).
- [41] G. Kresse and J. Furthmüller, *Physical Review B* **54**, 11169 (1996).
- [42] D. M. Ceperley and B. Alder, *Physical Review Letters* **45**, 566 (1980).
- [43] J. Perdew, *Phys. Rev. Lett.* **100**, 136406 (2008).
- [44] Y. Zhang, J. Sun, J. P. Perdew, and X. Wu, *Physical Review B* **96**, 035143 (2017).
- [45] S. Abrahams, S. Kurtz, and P. Jamieson, *Physical Review* **172**, 551 (1968).
- [46] X.-L. Wang, S. X. Dou, and C. Zhang, *NPG Asia Materials* **2**, 31 (2010).
- [47] M. Stengel, P. Aguado-Puente, N. A. Spaldin, and J. Junquera, *Physical Review B* **83**, 235112 (2011).
- [48] J. Fujioka, A. Doi, D. Okuyama, D. Morikawa, T. Arima, K. Okada, Y. Kaneko, T. Fukuda, H. Uchiyama, D. Ishikawa, et al., *Scientific Reports* **5**, 13207 (2015).
- [49] K.-H. Hellwege and A. Hellwege, *Landolt-Bornstein Table* (Springer, 1969).
- [50] A. M. Prokhorov and Y. S. Kuz’Minov, *Physics and chemistry of crystalline lithium niobate* (CRC Press, 1990).
- [51] H. H. Nahm and C. Park, *Applied Physics Letters* **78**, 3812 (2001).
- [52] K. F. Garrity, K. M. Rabe, and D. Vanderbilt, *Physical Review Letters* **112**, 127601 (2014).
- [53] P. Li, X. Ren, G.-C. Guo, and L. He, *Scientific Reports* **6**, 34085 (2016).
- [54] G. Rupprecht and R. Bell, *Physical Review* **135**, A748 (1964).

- [55] A. Mansingh and A. Dhar, Journal of Physics D: Applied Physics **18**, 2059 (1985).
- [56] B. Magyari-Köpe, S. G. Park, H.-D. Lee, and Y. Nishi, Journal of Materials Science **47**, 7498 (2012).
- [57] C. Lin, D. Shin, and A. A. Demkov, Journal of Applied Physics **117**, 225703 (2015).
- [58] M. Choi, F. Oba, and I. Tanaka, Applied Physics Letters **98**, 172901 (2011).
- [59] Y. Li, W. Schmidt, and S. Sanna, Physical Review B **91**, 174106 (2015).
- [60] G. G. DeLeo, J. L. Dobson, M. F. Masters, and L. H. Bonjack, Physical Review B **37**, 8394 (1988).
- [61] D. Smyth, Ferroelectrics **50**, 93 (1983).
- [62] K. Sweeney and L. Halliburton, Applied Physics Letters **43**, 336 (1983).

## Supplementary Materials

### Coexistence of polar displacements and conduction in doped ferroelectrics: an *ab initio* comparative study

#### I. DETAILS OF CRYSTAL STRUCTURES

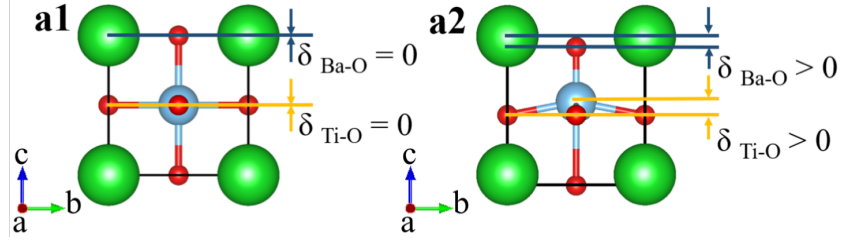


FIG. S1. Crystal structure of BaTiO<sub>3</sub> in rigid-band calculations. **a1**)  $Pm\bar{3}m$ . **a2**)  $P4mm$ .

Fig. S1 shows the crystal structure of BaTiO<sub>3</sub>. Panel **a1** shows zero Ba-O and Ti-O displacements in centrosymmetric BaTiO<sub>3</sub> (space group  $Pm\bar{3}m$ ), and it is the reference state. Panel **a2** shows non-zero Ba-O and Ti-O displacements in non-centrosymmetric BaTiO<sub>3</sub> (space group  $P4mm$ ). Ti-O displacement  $\delta_{\text{Ti-O}}$  is defined as:

$$\delta_{\text{Ti-O}} = z_{\text{Ti}} - \frac{1}{4} \sum_{i=0}^4 z_{\text{O}_i} \quad (\text{S1})$$

where  $z_{\text{O}_i}$  is the  $z$  position of the four nearest O atoms around a given Ti atom in  $xy$  plane. We note that in 119-atom cell, Ti#18 and Ti#23 that are closest to the oxygen vacancy have only three nearest O atoms.

Fig. S2 shows the crystal structure of LiNbO<sub>3</sub>. We show different bonding because we need different bondings to define  $\delta_{\text{Li-O}}$  and  $\delta_{\text{Nb-O}}$ . To define  $\delta_{\text{Li-O}}$ , we need the tetrahedron formed by one Li atom and three O atoms. For  $\delta_{\text{Nb-O}}$ , we need the octahedron with six oxygen atoms enclosing one Nb atom. Panels **a1** and **a3** show zero Li-O and Nb-O displacements in centrosymmetric LiNbO<sub>3</sub> (space group  $R\bar{3}c$ ), and it is the reference state. Panels **a2** and **a4** show non-zero Li-O and Nb-O displacements in non-centrosymmetric LiNbO<sub>3</sub> (space group  $R3c$ ). Li-O displacement  $\delta_{\text{Li-O}}$  is defined as:

$$\delta_{\text{Li-O}} = z_{\text{Li}} - \frac{1}{3} \sum_{i=0}^3 z_{\text{O}_i} \quad (\text{S2})$$

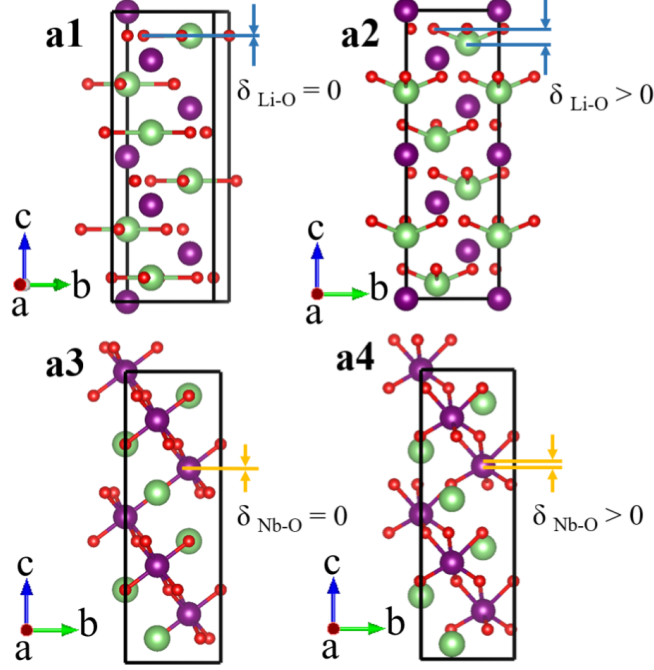


FIG. S2. Crystal structure of LiNbO<sub>3</sub> in rigid-band calculations. **a1)** and **a3)**  $R\bar{3}c$ . **a2)** and **a4)**  $R3c$ .

where  $Z_{O_i}$  is  $z$  position of the plane that is formed by the three nearest O atoms for a given Li atom. We note that in a 119-atom cell, Li#4 that is closest to the oxygen vacancy has only two nearest O atoms. Nb displacement  $\delta_{\text{Nb-O}}$  is defined as:

$$\delta_{\text{Nb-O}} = z_{\text{Nb}} - \frac{1}{6} \sum_{i=0}^6 z_{O_i} \quad (\text{S3})$$

where  $z_{O_i}$  is  $z$  position of the six nearest O atoms around a given Nb atom. We note that in a 119-atom cell, Nb#12 and Nb#24 that are closest to the oxygen vacancy have only five nearest O atoms.

## II. Ba-O CATION DISPLACEMENTS IN OXYGEN REDUCED $\text{BaTiO}_{3-\delta}$

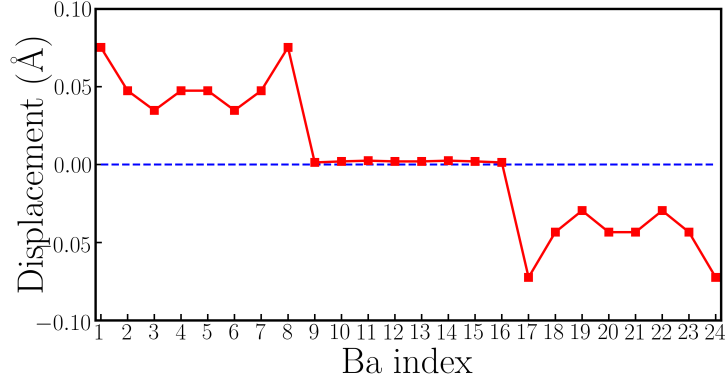


FIG. S3. Displacements along the  $z$ -axis of each Ba atom in oxygen reduced  $\text{BaTiO}_{3-\delta}$  from our supercell calculations.

FIG. S3 shows the Ba displacements along the  $z$ -axis in the 119-atom  $\text{BaTiO}_3$  supercell with an oxygen vacancy. It is noticed that there is no net average Ba displacement in electron-doped  $\text{BaTiO}_3$  from our supercell calculations. The polar displacements on Ba atoms #1 and #24 (#8 and #17 etc.) are of the same magnitude but opposite in direction. These are caused by the presence of the oxygen vacancy.

### III. COMPARISON OF LDA AND PBEsol CALCULATIONS

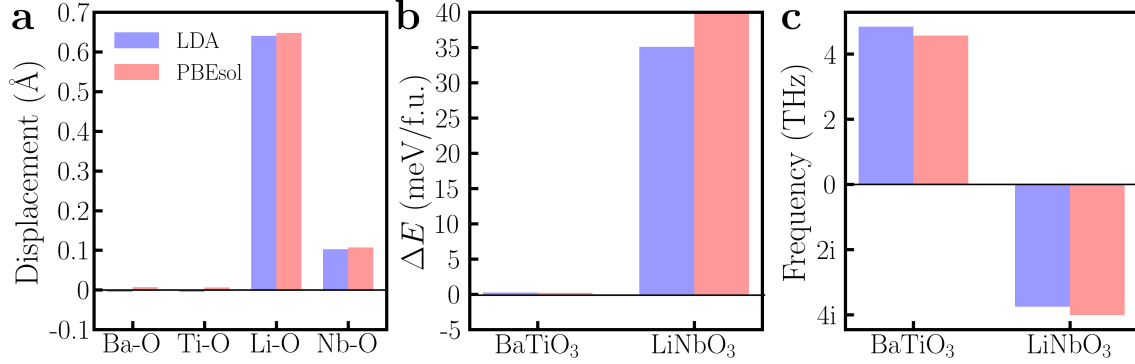


FIG. S4. Comparison of LDA and PBEsol calculations on the key results. Panel **a)** Ba-O, Ti-O, Li-O and Nb-O cation displacements in non-centrosymmetric structures of BaTiO<sub>3</sub> and LiNbO<sub>3</sub> with 0.3e/f.u. doping concentration. Panel **b)** Energy difference between the centrosymmetric and non-centrosymmetric structures of BaTiO<sub>3</sub> and LiNbO<sub>3</sub> with 0.3e/f.u. doping concentration. Panel **c)** phonon frequency of the zone-center ferroelectric mode of cubic BaTiO<sub>3</sub> and  $R\bar{3}c$  LiNbO<sub>3</sub> with 0.3e/f.u. doping concentration.

We check our key results using PBEsol and find no significant changes. The comparison between LDA and PBEsol results is shown in FIG. S4. Ba-O and Ti-O displacements are completely suppressed upon 0.3e/f.u. doping, while Li-O and Nb-O displacements are still significant at the same level of electron doping. At 0.3e/f.u. doping, the centrosymmetric and non-centrosymmetric structures are essentially the same for BaTiO<sub>3</sub> but are distinct for LiNbO<sub>3</sub>. Our results are robust against different exchange correlation.

#### IV. COMPARISON OF TWO TYPE ELECTRONS IN OXYGEN REDUECED $\text{BaTiO}_{3-\delta}$ AND $\text{LiNbO}_{3-\delta}$

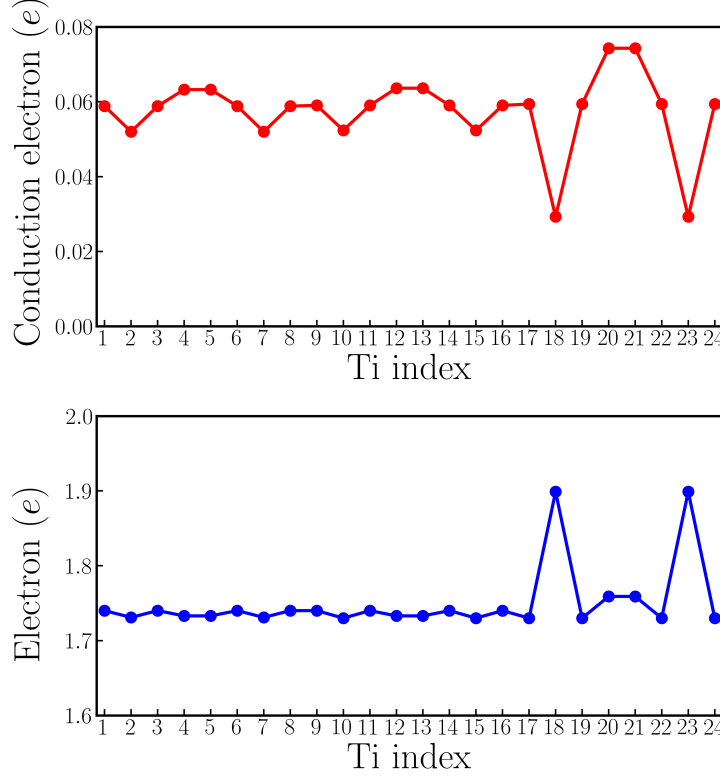


FIG. S5. **a)** The number of conduction electrons in Ti- $d$  states on each Ti atom by integrating Ti- $d$  states from the band gap to the Fermi level. **b)** The number of atomic Ti- $d$  electrons of each Ti atom by integrating Ti- $d$  electrons in a spherical region. Both results are obtained from a 119-atom  $\text{BaTiO}_3$  supercell calculation.

Fig. S5 compares two types of Ti- $d$  electrons in 119-atom  $\text{BaTiO}_3$  supercell with an oxygen vacancy. The upper panel shows the Ti- $d$  conduction electrons which are obtained by integrating the Ti- $d$  states from the band gap to the Fermi level. The lower panel shows the atomic Ti- $d$  electrons that are obtained by integrating charge density in a spherical region. Atomic Ti- $d$  electrons include both Ti- $d$  electrons in the conduction bands (which are above the band gap) and Ti- $d$  electrons in the valence bands (which are below the band gap). The Ti- $d$  electrons in the valence bands are due to strong hybridization between Ti- $d$  and O- $p$  states [S1]. From Fig. S5, we find that indeed the two nearest-neighbor Ti atoms have the largest number of Ti- $d$  electrons. However, not all these electrons are in the



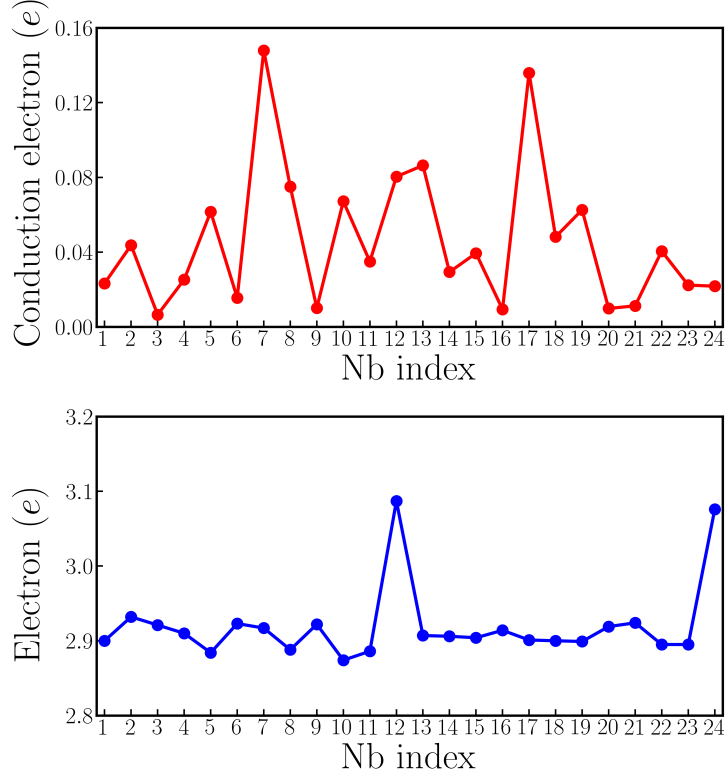


FIG. S6. **a)** The number of conduction electrons in Nb- $d$  states on each Nb atom by integrating Nb- $d$  states from the band gap to the Fermi level. **b)** The number of atomic Nb- $d$  electrons of each Nb atom by integrating Nb- $d$  electrons in a spherical region. Both results are obtained from a 119-atom  $\text{LiNbO}_3$  supercell calculation.

conduction bands.

Fig. S6 compares two-types of Nb- $d$  electrons in 119-atom  $\text{LiNbO}_3$  supercell with an oxygen vacancy. Electron distribution in  $\text{LiNbO}_3$  is similar to that in  $\text{BaTiO}_3$ . Nb #12 and Nb#24 have the most Nb- $d$  electrons (Fig. S6 **b**), but their conduction electrons are not necessarily the most (Fig. S6 **a**).

## V. CALCULATIONS OF OXYGEN REDUCED $\text{BaTiO}_{3-\delta}$ USING LDA+ $U$ OR LARGER SUPERCELL

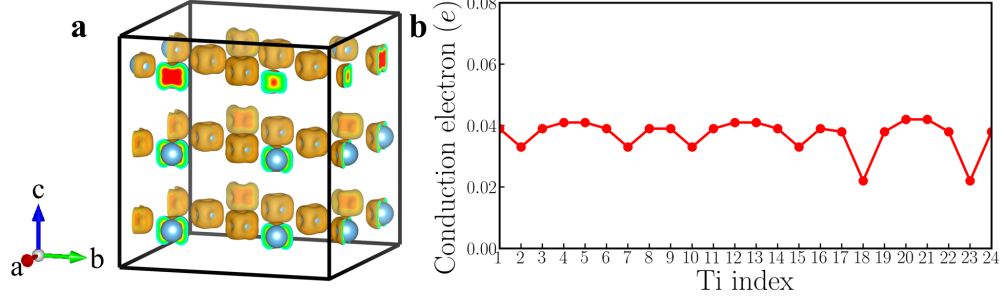


FIG. S7. LDA+ $U$  supercell calculations of electron doped  $\text{BaTiO}_3$ . Panel **a**) an iso-value surface of conduction electron distribution in oxygen reduced  $\text{BaTiO}_{3-\delta}$  with  $\delta = 4.2\%$ . Panel **b**) conduction electrons on each Ti atom in the 119-atom cell by integrating Ti- $d$  states from band gap to the Fermi level.

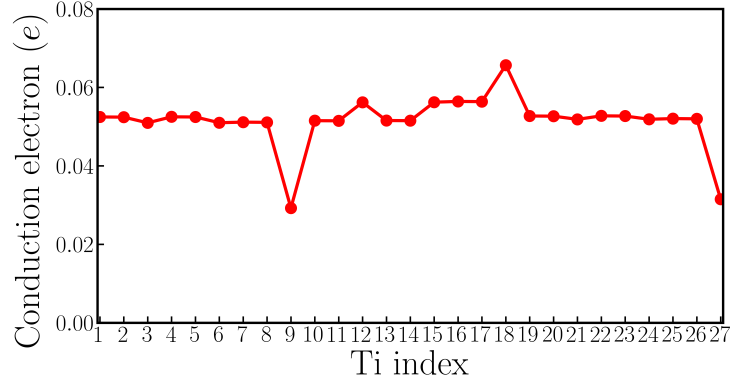


FIG. S8. Conduction electron on each Ti atom in the 134-atom  $\text{BaTiO}_3$ . The number of conduction electron on each Ti atom is obtained by integrating Ti- $d$  states from band gap to the Fermi level.

We check oxygen reduced  $\text{BaTiO}_3$  using LDA+ $U$  method (with  $U_{\text{Ti}} = 4$  eV). The new results are shown in Fig. S7. Panel **a** shows the iso-value surface of Ti- $d$  conduction electrons on Ti sites and panel **b** shows the number of Ti- $d$  conduction electrons on each Ti atom in oxygen reduced  $\text{BaTiO}_{3-\delta}$ . From LDA+ $U$  calculations, we find Ti- $d$  conduction electrons are still homogeneously distributed.

We also test the cell size by calculating conduction electrons on each Ti atom in the 134-atom  $\text{BaTiO}_3$  supercell. The new result is shown in Fig. S8. Conduction electron

distribution in Ti- $d$  states is homogeneous in a 134-atom BaTiO<sub>3</sub> cell, similar to 119-atom cell calculation.

## VI. CALCULATIONS OF OXYGEN REDUCED $\text{LiNbO}_{3-\delta}$ WITH A HIGHER DOPING CONCENTRATION

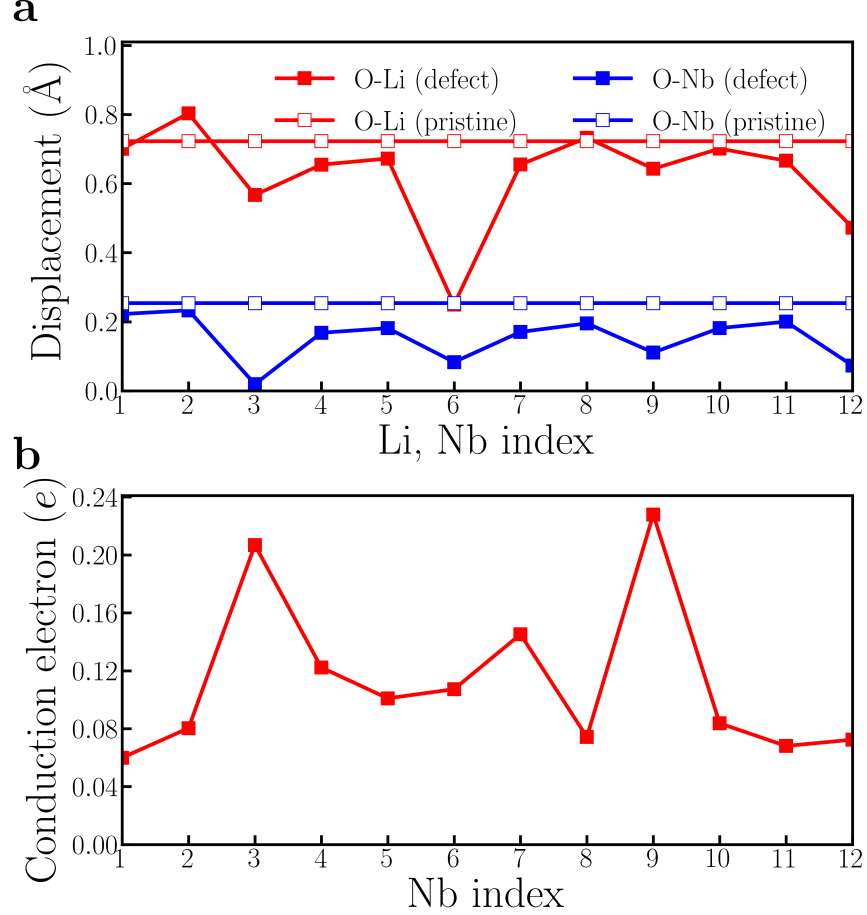


FIG. S9. Panel **a**) Polar displacements of each Li (red square) and Nb atom (blue square) in oxygen reduced  $\text{LiNbO}_{3-\delta}$  with  $\delta = 8.4\%/f.u.$ . The solid squares are calculated from the 59-atom cell. The open squares are bulk  $\delta_{\text{Li-O}}$  and  $\delta_{\text{Nb-O}}$  of pristine  $\text{LiNbO}_3$ . Panel **b**) Conduction electrons on each Nb atom in the 59-atom cell.

FIG. S9a shows  $\delta_{\text{Li-O}}$  for each Li atom and  $\delta_{\text{Nb-O}}$  for each Nb atom in oxygen reduced  $\text{LiNbO}_{3-\delta}$  with  $\delta = 8.4\%/f.u.$  FIG. S9b shows the number of conduction electrons on each Nb atom in 59-atom  $\text{LiNbO}_3$  supercell. The number of conduction electrons on each Nb atom is obtained by integrating Nb-d states from band gap to the Fermi level. Li#4, Nb#6 and Nb#12 are closest to the oxygen vacancy in 59-atom  $\text{LiNbO}_3$  cell. The minimum conduction electron in 59-atom  $\text{LiNbO}_3$  is  $0.06e$ , which is much larger than that in 119-atom  $\text{LiNbO}_3$

supercell, only  $0.0065e$ .

## VII. OXYGEN REDUCED $\text{LiNbO}_{3-\delta}$ WITH TWO OXYGEN VACANCIES

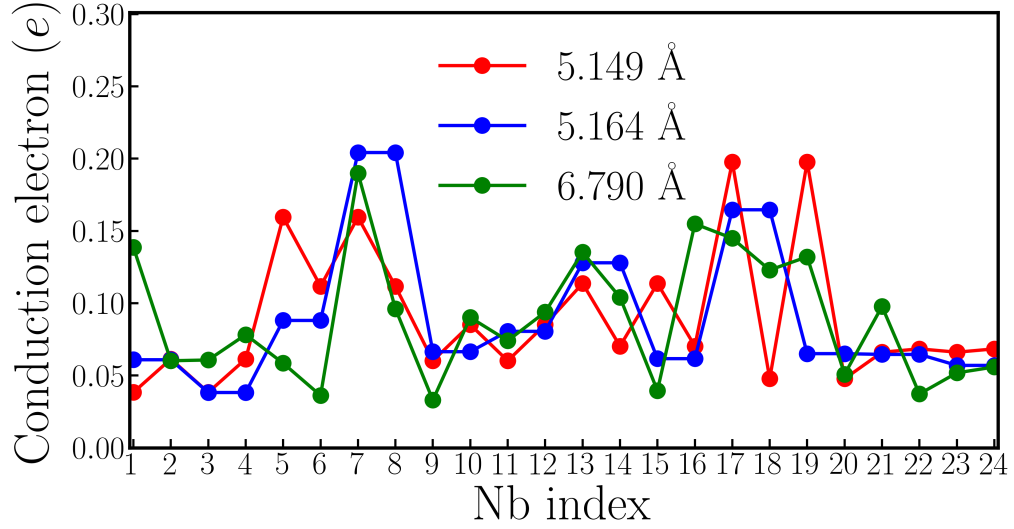


FIG. S10. Distribution of conduction electrons in Nb- $d$  states from three different configurations of a 118-atom cell that includes two oxygen vacancies.

We introduce two oxygen vacancies into a 120-atom  $\text{LiNbO}_3$  supercell and study conduction electron distribution in these cells with different vacancy distances. These results are shown in FIG. S10. For all three separations, conduction electrons on Nb atoms are inhomogeneously distributed.

---

\* Correspondence to hanghui.chen@nyu.edu or yuechen@hku.hk.

[S1] C. Marianetti, G. Kotliar, and G. Ceder, Physical Review Letters **92**, 196405 (2004).